Turkish Journal of Science & Technology
17(2), 375-394, 2022

Research Paper
https://doi.org/10.55525/tjst.1080861

Improving the Flux-Weakening Capability of Interior Permanent Magnet Machines by Number of Turns Changing Methodology

Tayfun GÜNDOĞDU[1*]
Department of Electrical and Electronic Enginnering, Faculty of Engineering, Hakkari University, Hakkari, Turkey
[*1] tayfungundogdu@hakkari.edu.tr

(Geliş/Received: 01/06/2022; Kabul/Accepted: 20/08/2022)

Abstract: In this paper, an interior permanent magnet (IPM) machine having two sets of windings with different number of turns is developed to improve the limited flux-weakening (FW) capability and efficiency, simultaneously. The flux-adjustable range appears to be somewhat limited because of the limited maximum inverter voltage and high magnetic saturation, which degrades the FW capability. To address its restricted FW capability, a unique winding-switching concept is introduced, in which auxiliary coils with lower turns alternately function as the secondary armature winding, resulting in flux-linkage reduction within the same phase. Winding topologies, design considerations, the FW principle, and FW computations have all been addressed. To validate the feasibility of the proposed FW enhancement strategy, a co-simulation procedure based on the 2D finite element method (FEM) and MatLab codes is used to determine the steady-state and FW performance characteristics of IPM machines with various winding topologies. All steady-state and FW performance characteristics of the conventional IPM machine and the proposed IPM machines have been compared quantitatively. Furthermore, to ensure the accuracy of the analytical and numerical calculations provided in this study, the predicted efficiency map of the original Toyota Prius 2010 IPM machine is validated using the efficiency measurements provided.

Key words: Flux-weakening capability, IPM machines, winding switching method, turn number variation, efficiency map.

Gömülü Tip Mıknatıslı Makinaların Sipir Sayısı Değiştirme Metodolojisi ile Akı Zayıflatma Kapasitesinin Geliştirilmesi

Öz: Bu çalışmada, sınırlı akı zayıflatma (AZ) kapasitesi ve verimi aynı anda arttırabilmek için farklı sipir sayılarına sahip birbirinden izole iki adet sargısı olan bir gömülü tip kalıcı mıknatıslı (IPM) makina geliştirilmiştir. Akı ayarlayabilme aralığı, AZ kapasitesini düşüren sınırlı maksimum inverter gerilimi ve yüksek manyetik doygunluk nedeniyle sınırlanmaktadır. Kısıtlı AZ kabiliyetini geliştirmek için, ana sargıya göre daha düşük sipir sayısına sahip yardımcı bobinlerin sistematik olarak anahtarlanması ile akı bağlantısının azalmasını sağlayan benzersiz bir sarım-anahtarlama konsepti tanıtılmıştır. Sargı topolojileri, tasarım hususları, AZ ilkesi ve hesaplamaları tümüyle ele alınmıştır. Önerilen AZ kapasitesi geliştirme stratejisinin uygulanabilirliğini doğrulamak için, çeşitli sargı topolojilerine sahip IPM makinelerinin kararlı durum ve AZ performans özelliklerini belirlemek için 2-boyutlu sonlu elemanlar yöntemine (SEY) ve MatLab kodlarına dayalı bir ortak simülasyon prosedürü kullanılmıştır. Klasik ve önerilen IPM makinalarının tüm kararlı durum ve AZ performans özellikleri nicel olarak karşılaştırılmıştır. Ayrıca, bu çalışmada sağlanan analitik ve sayısal hesaplamaların doğruluğunu sağlamak için, orijinal Toyota Prius 2010 IPM makinasının öngörülen verimlilik haritası, sağlanan verimlilik ölçümleri kullanılarak doğrulanmıştır.

Anahtar kelimeler: Akı zayıflatma kapasitesi, IPM makinalar, sargı değiştirme yöntemi, sipir sayısı değişimi, verim haritası.

1. Introduction

Permanent magnet synchronous machines (PMSMs) have gained popularity in recent years due to their benefits such as high efficiency, high torque density, high torque to current ratio, low weight, and high-power factor. The PMSMs are especially well-suited for the use of electric vehicle (EV) and traction applications in order to reduce system volume and weight. In most EVs, a battery is employed as an energy storage and power source, with a limited output voltage. A direct drive system replaces the gear box to reduce energy loss. As a result, PMSMs are typically required to operate at high speed and flux-weakening (FW) regions, particularly in traction systems.

Inability to adjust the fixed PM field limits PMSM applications at constant-power operating ranges [1]. To provide a wide speed range, a large minus *d*-axis current is required to generate demagnetizing magnetic flux. This

[*] Corresponding author: tayfungundogdu@hakkari.edu.tr. ORCID Number of the author: 0000-0002-7150-1860,

demagnetizing magnetic flux cancels out some of the reversible magnetic flux produced by PMs. The effective air gap magnetic flux is lowered, and the PMSM speed range is widened [1], [2].

Flux weakening control techniques are frequently used to drive the PMSMs and to increase the speed range. However, due to inverter constraints on maximum current and voltage [1]–[6], the speed range may be constrained and unsuitable for some applications, such as EV. Furthermore, the FW obtained with this technique raises the risk of irreversible PM demagnetization and copper losses in the windings. As a consequence, variable flux concepts have been established [7] for improved flux weakening capabilities and enhanced speed range expansion while maintaining high efficiency. The PM flux level can be regulated via electrical, mechanical, or other approaches to broaden the speed range and enhance the PMSMs' flux weakening capabilities. Many hybrid excitation machines, or PM machines with electrical or mechanical variable flux techniques, have been developed during the past 15 years [8–20]. IPM, homopolar and bipolar embedded PM, hybrid excited, consequent pole PM, and other synchronous PM devices are all subject to the same flux control paradigm [12]–[19]. In the axial flux surface-mounted PM machines presented in [21, 22], the PM flux-linkage is adjusted by the relative movement of two separate windings. Radial flux surface-mounted PM machines can be altered to be capable of changing the PM flux linkage by splitting the rotor into two separate portions [23]. Similarly, the interior PM machine's flux barriers can be filled with movable ferromagnetic material fragments to modify the PM flux-linkage while it is in operation [24–26]. Moreover, the doubly salient machine makes use of moveable ferromagnetic parts that are outside of the stator to create a short-circuit route for the PM flux [27]. Memory motors [28], another type of variable flux machine, have been proposed as using several flux weakening methods. The use of AlNiCo magnets, which can be magnetized and demagnetized with a short current pulse in the d-axis direction, enables for the modification of PMs remanence, allowing for flux weakening and strengthening during machine operation [29–32]. Furthermore, by adjusting the winding connection or the number of turns per phase, the pole-changing and double-winding set machines enable variable flux capability [33], [34]. Basically, PM machines have pioneered the concept of winding switching or altering, such as the wye/delta transformation [33].

Winding switching is the most basic, low-cost, and adaptable of the methods discussed above. However, it frequently needs machine rewinding, which raises the cost. The requirement for more switches, gating circuits, and a more complex control board raises the cost of the drive. The switching transient (torque, current, and/or voltage pulsations), which might damage the stator windings or inverter, is another drawback of this method. Several research [33–36] have addressed this issue and proved the feasibility of winding changeover during machine operation. In addition, it has been shown that the high-pulsations in voltage or current can be eliminated by implementing a zero-crossing voltage or current control method [37], [38].

This research attempted to provide a unique winding-switching/changing concept, corresponding to the change of phase winding groups with a different number of turs, in order to improve the IPM machine's limited FW capability and overall efficiency, simultaneously. To change the machine's operating mode, two independent winding groups per phase, namely main and auxiliary windings with differing number of turns, have been created and functionally switched. As a consequence, high-speed back EMF will be decreased, reducing the inverter rating required and extending the available adjustable speed range. Thanks to the proposed winding switching mechanism, three different operating modes, namely constant torque (highest-torque) mode, moderate FW mode, and deep FW (highest-speed) mode, are achieved. The physical and operating specifications of the Toyota Prius 2010 IPM machine were employed as key design parameters. The winding topologies, design considerations, the FW principle, and the FW computations have all been addressed. In order to confirm the feasibility of the proposed FW enhancement technique, a co-simulation algorithm, consisting of the 2D finite element method (FEM) and MatLab, is employed to calculate the steady and flux-weakening performance of the IPM machines having different winding topologies. The steady-state characteristics listed below have been investigated and compared for different switching modes:

- Harmonic analysis of air gap flux density waveform;
- Harmonic analysis of flux linkage waveform;
- Harmonic analysis of Back-EMF waveform;
- Electromagnetic torque waveform;
- Machine losses and efficiency;
- Flux density and flux line distributions.

As for the FW characteristics the followings have been investigated and compared for different switching modes:

- Torque-speed curves;
- Power-speed curves;
- Efficiency maps;

- Inverter current-speed and voltage-speed curves.

Finally, to be able to validate the numerical and analytical calculations, the predicted efficiency map of the original Toyota Prius 2010 IPM machine is verified through the efficiency measurements provided by [39].

2. Number of Turns Changing (Winding-Switching) Concept

A double-fed IPM machine is proposed in [40] to achieve improved FW characteristics. It has been reported that the obtained FW and efficiency characteristics of the dual-fed IPM machine is satisfactory. Although the winding topology proposed in [40] is similar to the winding topology proposed in this study, it requires two separate inverters to supply the windings. Although the winding topology proposed in [40] is similar to the winding topology proposed in this study, it requires two separate inverters to supply the windings. Therefore, the cost of the FW enhancement approach described in [40] is much greater than the cost of the method described in this work.

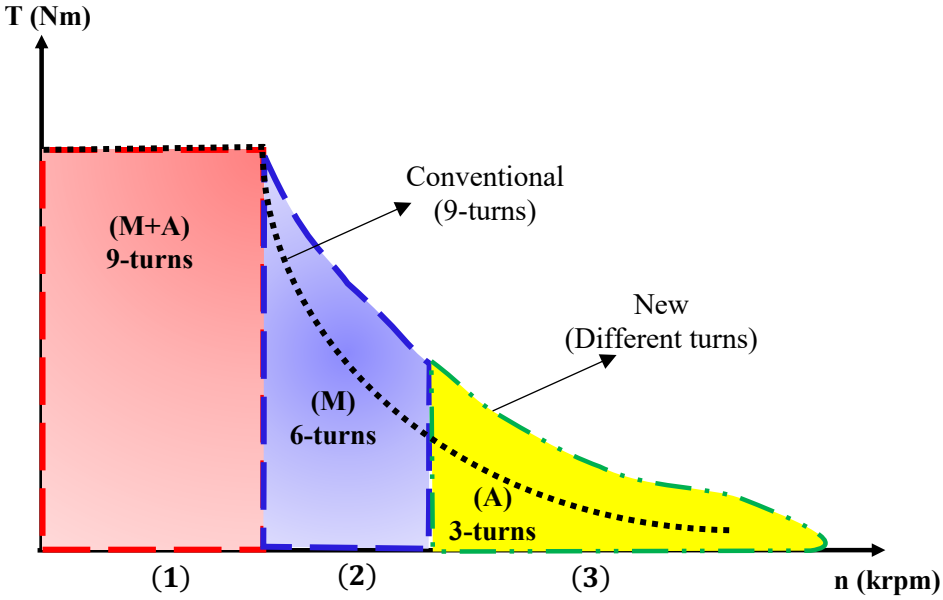

Figure 1. Principle torque-speed curve showing the improved FW characteristic.

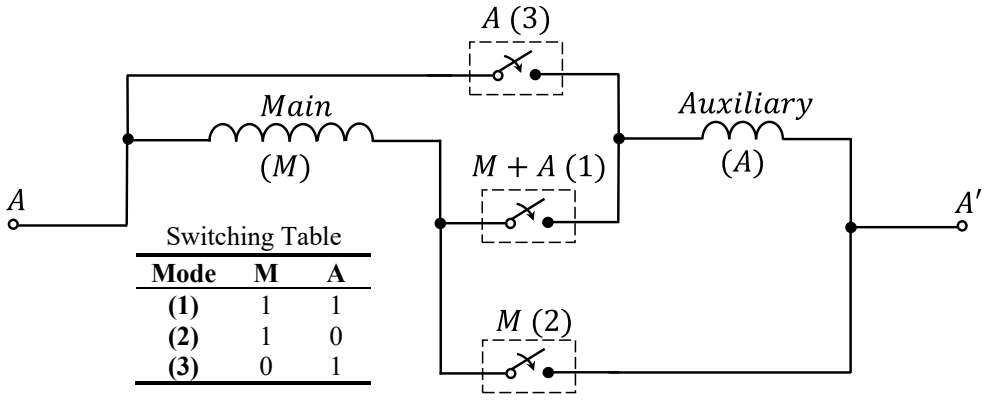

Switching Table

Mode	M	A
(1)	1	1
(2)	1	0
(3)	0	1

Figure 2. One phase connection diagram of main and auxiliary windings according to their switching order.

Instead of utilizing additional inverters, it requires electronic switches such as IGBT in order to change the turn number per phase during the operation. The basic principle is that to be able to weaken the main flux, the number of turns has been reduced instead of producing an additional opposite-direction flux. The principle torque-speed curve and corresponding winding connection diagram are shown in Figure 1 and Figure 2, respectively. Considering the switching table shown in Figure 2, three different operating modes can be achieved. Once both windings are activated (case#1), the machine operates at constant torque region. If only the main winding is

activated (case#2), the machine operates at moderate torque/speed region. Alternatively, if only the auxiliary winding is activated (case#3), the machine operates at deep FW region.

Some key advantages of the turn-changing concept are presented as follows:

- ✓ Does not require an additional inverter;
- ✓ Does not consume power to weaken the flux;
- ✓ Does not produce additional copper loss;
- ✓ Depending on the number of turn shares of the main and auxiliary windings, it is possible to increase the power up to the maximum limits of the inverted at the very-high speed operations.

3. Design Specifications and Analysis Method

In this section, to be able to verify the calculations, the number of turns chancing method has been directly utilized for the original IPM machine design. To examine the effects of various turning sharing between the main and auxiliary windings, a M/A: 8/3 and a M/A: 7/4 version of Toyota Prius IPM machine are designed. M/A: 8/3 indicates that turn-changing IPM machine with 8-turns for main winding and 3-turns for auxiliary windings. In the similar manner, the M/A: 7/4 indicates that the main windings have 7-turns and the auxiliary windings have 4-turns. The total turn number per phase, which is 11-turns, kept the same for all the designs. The design specifications of the considered machines are listed in Table 1 and the cross-sectional views of the machines are shown in Figure 3. The coefficients of flux linkage, inductance, and power loss were estimated parametrically using 2D, non-linear, time-stepping FEM. Using the hybrid FW control approach, these parameters are entered into a MatLab program for analytical FW computation.

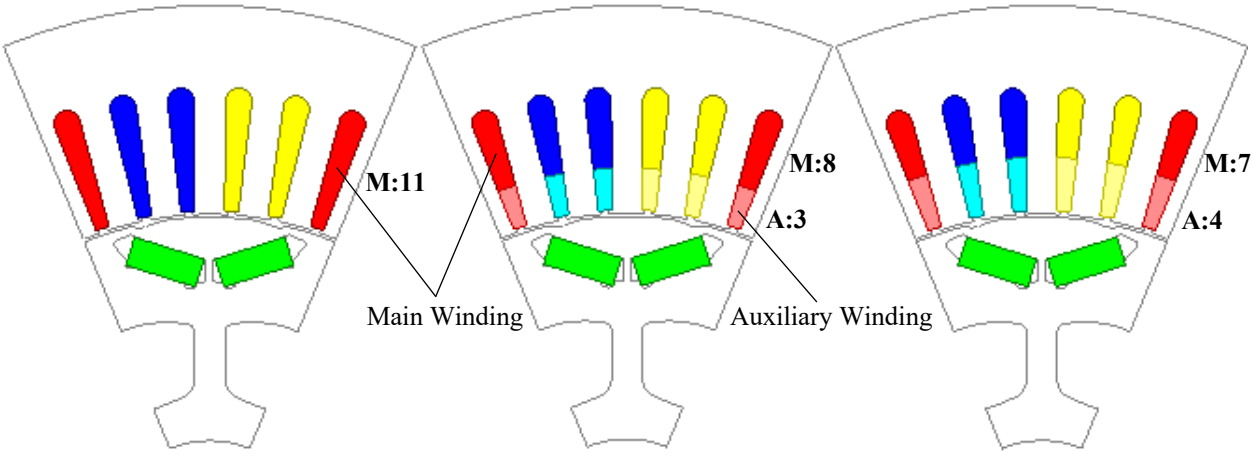

(a) Original (ORG) (b) M/A: 8/3 (c) M/A: 7/4

Figure 3. 2-D cross-sectional views of the original and proposed IPM machines with turn changing topology.

One of the main limitations of IPM drives is the restricted excitation. When the inverter's voltage limit u_{max} is reached, as shown in Equation (1), the back-EMF of the IPM machine rises with rotor speed in the constant-torque region. Equation (2) states that the machine rating limits the maximum current (i_{max}), whereas the inverter rating limits the maximum voltage. The corresponding d- and q-axis voltages are expressed in Equations (3) and (4), respectively. Usually, the operating mode of a machine is determined according to the base speed n_b (see Equation (5)) of the machine. As a result, the control approach is relatively straightforward: the maximum torque per ampere (MTPA) technique is used to control the machine if it operates below the base speed. Moreover, if it exceeds the base speed, then it is controlled by the FW control algorithm, which searches for the optimal current angle γ, delivering the maximum torque available. Furthermore, the correlation between the electromagnetic torque T_e and γ is expressed in Equation (6).

$$V_d^2 + V_q^2 \leq u_{max}^2 \tag{1}$$

$$i_d^2 + i_q^2 \leq i_{max}^2 \tag{2}$$

$$V_d = R_s i_d - \omega_s L_q i_q \tag{3}$$

$$V_q = R_s i_q + \omega_s \left(L_d i_d + \lambda_{pm}\right) \tag{4}$$

$$n_b = \frac{120}{2\pi P} \frac{u_{max}}{\sqrt{\left(\lambda_{pm} - L_d i_d\right)^2 + \left(L_q i_q\right)^2}} \tag{5}$$

$$T_e = 0.5P\left[\lambda_{pm} i_s \cos\gamma + 0.5\left(L_d - L_q\right) i_s^2 \sin 2\gamma\right] \tag{6}$$

In Equations between (1) and (6); V_d, V_q, i_d, i_q, L_d, and L_q are the voltage, current, and inductance of d- and q-axes, respectively. R_s, i_s, ω_s, λ_{pm}, and P are the phase resistance, current vector, angular speed, flux linkage of PMs, and pole number, respectively. For the FW calculations, the dq equivalent circuit of the IPM machine is employed. More details about the FW algorithm employed in this study can be found in [41].

Table 1 Design Specifications

Parameter	**unit**	**ORG**	**M/A: 8/3**	**M/A: 7/4**
Stator Outer Diameter	mm	264		
Stator Inner Diameter	mm	161.9		
Stator axial length	mm	50.8		
Rotor Inner Diameter	mm	51		
Air-gap	mm	0.73		
Number of Slot		48		
Turns per coil		11	8+3	7+4
Parallel brunches		1		
Coils in series per phase		8	8+8	8+8
Number of turns per phase		88	64+24	56+32
Slot fill factor		0.448		
Stator slot height	mm	26.753		
Stator tooth width	mm	7.55		
Stator slot radius	mm	3.447		
Stator slot opening width	mm	1.9		
Stator slot opening height	mm	0.85		
Outer bridge thickness (Ribs)	mm	1.836		
Inner bridge thickness	mm	1.863		
O1 (length of the PM positions to origin)	mm	63.141		
B1 (length between the PMs on q)	mm	12.806		
PM dimensions (W× T)	mm^2	17.88065×7.16		
Core Material		Steel 1010		
Hysteresis loss coefficient (K_h)		179.04		
Classical loss coefficient (K_c)		0.375		
Excess loss coefficient (K_e)		0.262		
Mass density (ρ)	kg/m^3	7650		
Stacking factor (K_{fe})		0.93		
PM material		NdFeB35		
Permeability		1.05		
Conductivity (σ)	s/m	625000		
Coercivity (H_c)	A/m	-932193.2381		
Mass density ρ	kg/m^3	7400		

4. Steady-State Performance Characteristics at Full Load

The steady-state analyses of the considered machines are presented as follows. To be able to find the ideal current angle γ delivering the maximum time-averaged torque, parametric analyses, including variations of d and q axes currents, flux linkages, and torque, have been performed, and the results are illustrated in Figure 4. It can be observed that the maximum torque is achieved at 45°.

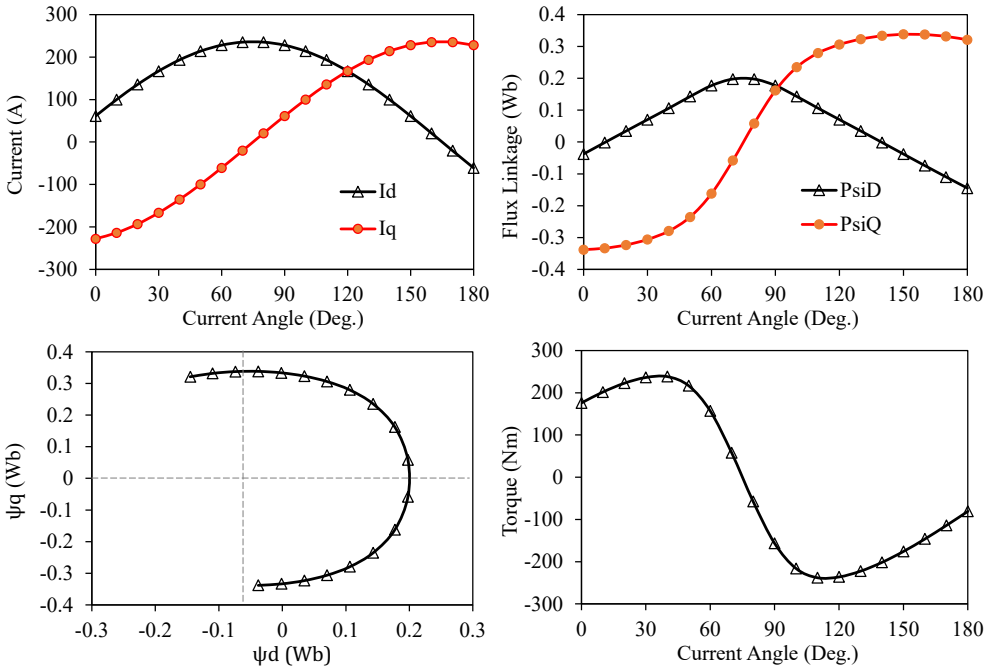

Figure 4. Determination of the optimal current angle for full load analyses.

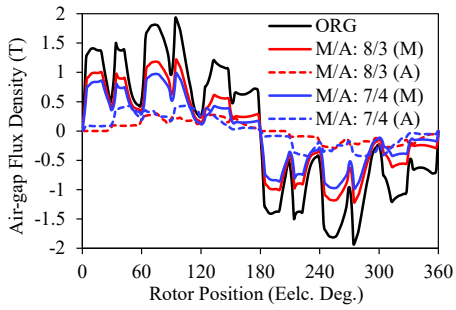

(a)

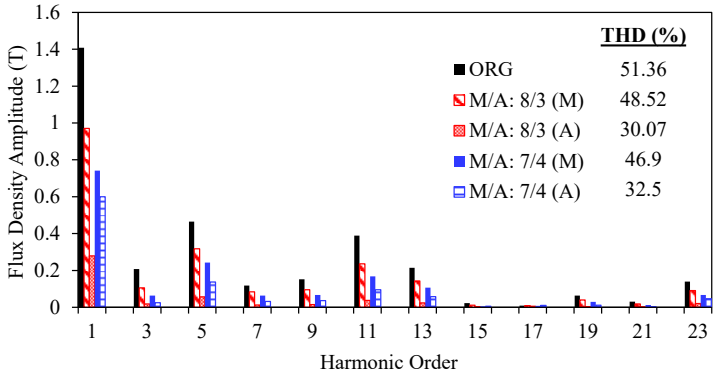

(b)

Figure 5. Air-gap flux density distributions and their harmonic spectra.

The results of the harmonic analysis of the air-gap flux density waveform illustrated in Figure 5. As clearly seen, the amplitude of the flux density changes as a function of turn number. As expected, the original design 'ORG' with 11-turns per slot has the highest air-gap flux density, whilst the turn-changing design with 3-turns 'M/A: 8/3 (A)' has the lowest air-gap flux density amplitude. Note that the numbers inside of the brackets indicate the number of turns for the main 'M' and auxiliary 'A' windings, respectively. The waveform distortion levels are fairly severe, as can be observed from the waveforms, due to the combined influence of the winding MMF harmonics and the slotting effect.

The harmonic analysis results of the flux-linkage waveforms are shown in Figure 6. As expected, the ORG design has the highest flux-linkage amplitude while M/A: 8/3 (A) has the lowest. Therefore, it is conceivable to forecast how each design will function in the high-speed operating region by taking into account these flux-linkage amounts. It is clear that windings with fewer turns provide more torque and, as a result, more power in the deep FW region.

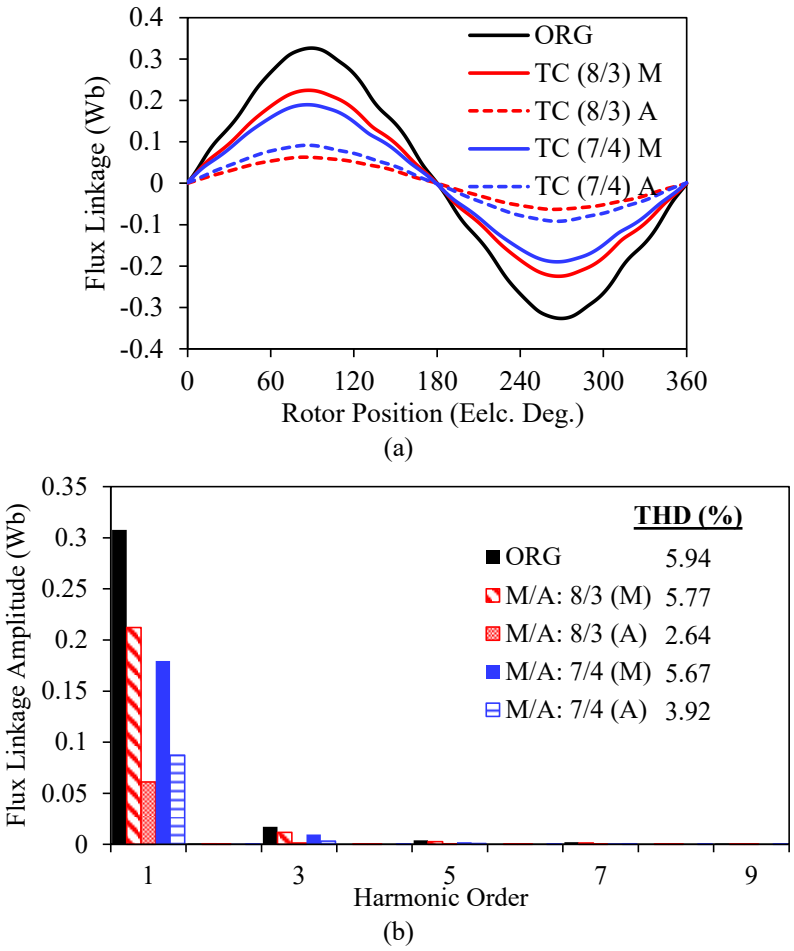

Figure 6. Flux-linkage waveforms and their harmonic spectra.

Figure 7 depicts phase 'A' back-EMF waveforms and harmonic spectra. When the air-gap flux density, flux-linkage, and back-EMF fundamental amplitudes are compared, it is clear that they have a fixed ratio dependent on the number of rotations. Figure 8 depicts the torque fluctuation with regard to rotor position. Given this figure, it is clear that if the Prius IPM machine is constructed with 8-turn main and 3-auxiliary turns (M/A: 8/3), the acquired torque in the deep FW area will be lower than that of the design with 7-turn main and 4-auxiliary turns (M/A: 7/4).

Figure 9 shows a comparison of the power losses of the considered IPM machines. The copper loss is the main loss component at 1000rpm and 236A operation conditions, as seen in the figure. Furthermore, the power loss levels vary based on the output power of the machines with varying rotations. The higher the power, the greater the loss, as expected.

The flux density and flux line distributions of the IPM machines for various operating modes (at different magnetization states) are illustrated in Figure 10 and Figure 11, respectively. As seen in the figures, as the number of turns is lowered, the induced voltage and flux-linkage are reduced, as is the machine's saturation level. It is also clear that as the number of spins is reduced, so are the flux lines traveling through the stator slots. The effective flux linkage fluctuates with the switched winding, which is mostly resulted in the substantial magnetic saturation of the stator teeth and rotor flux barrier bridges.

Table 2 summarizes the comparison of the steady-state performance characteristics of the original and proposed IPM machines.

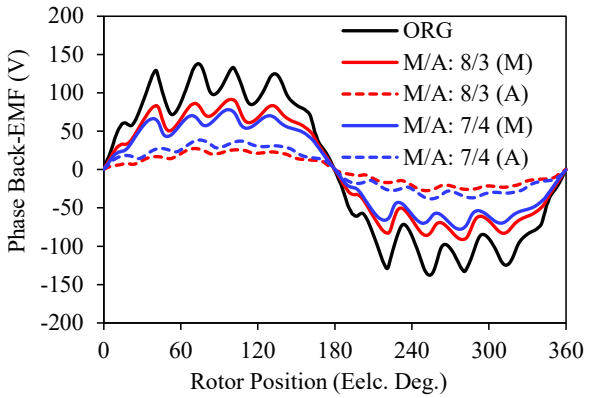

(a)

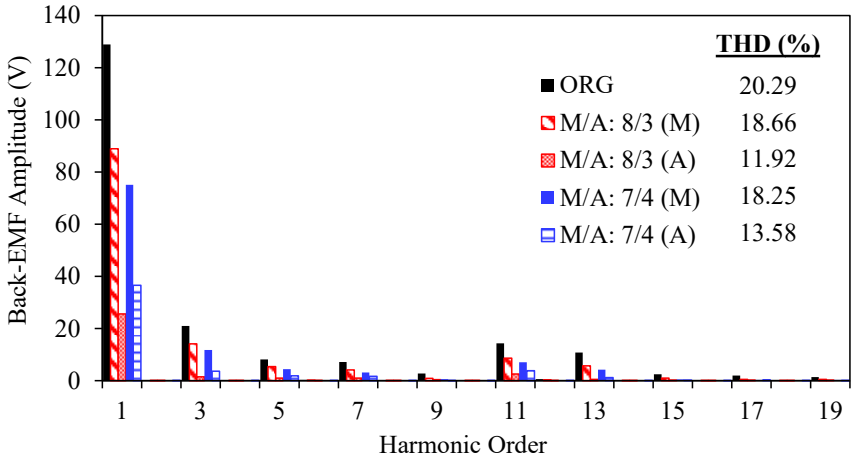

(b)

Figure 7 Phase 'A' back-EMF waveforms and their harmonic spectra.

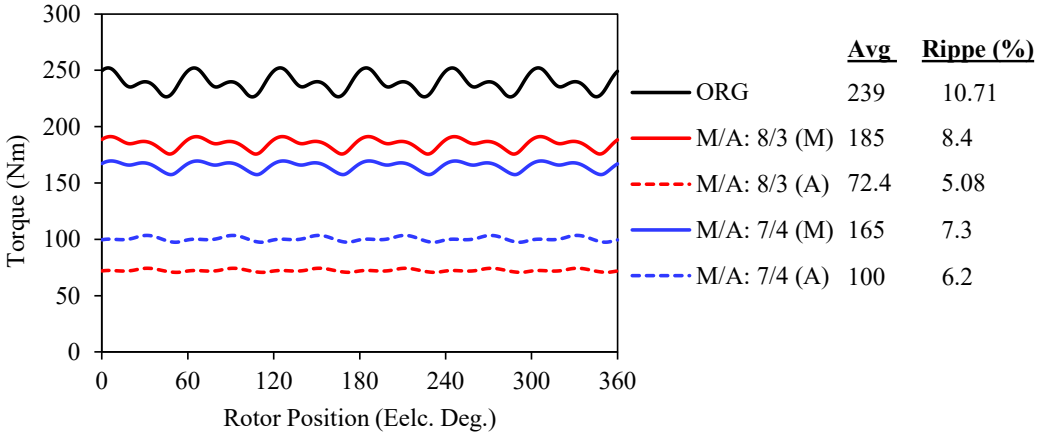

Figure 8 Torque against rotor position.

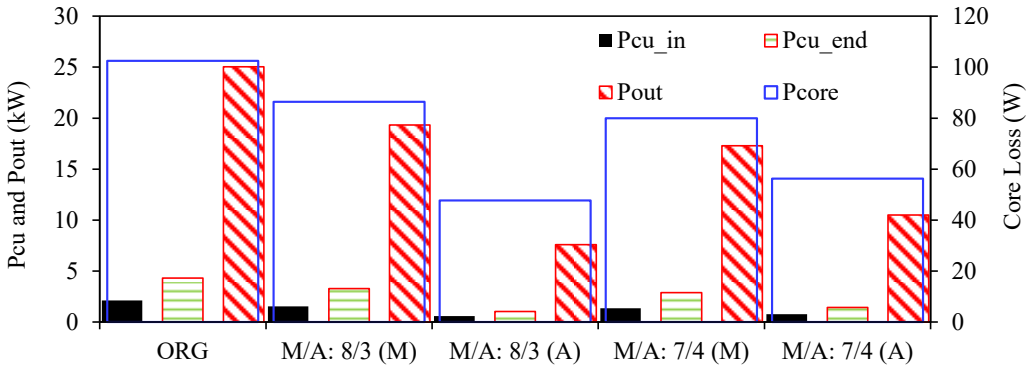

Figure 9 Comparison of power losses.

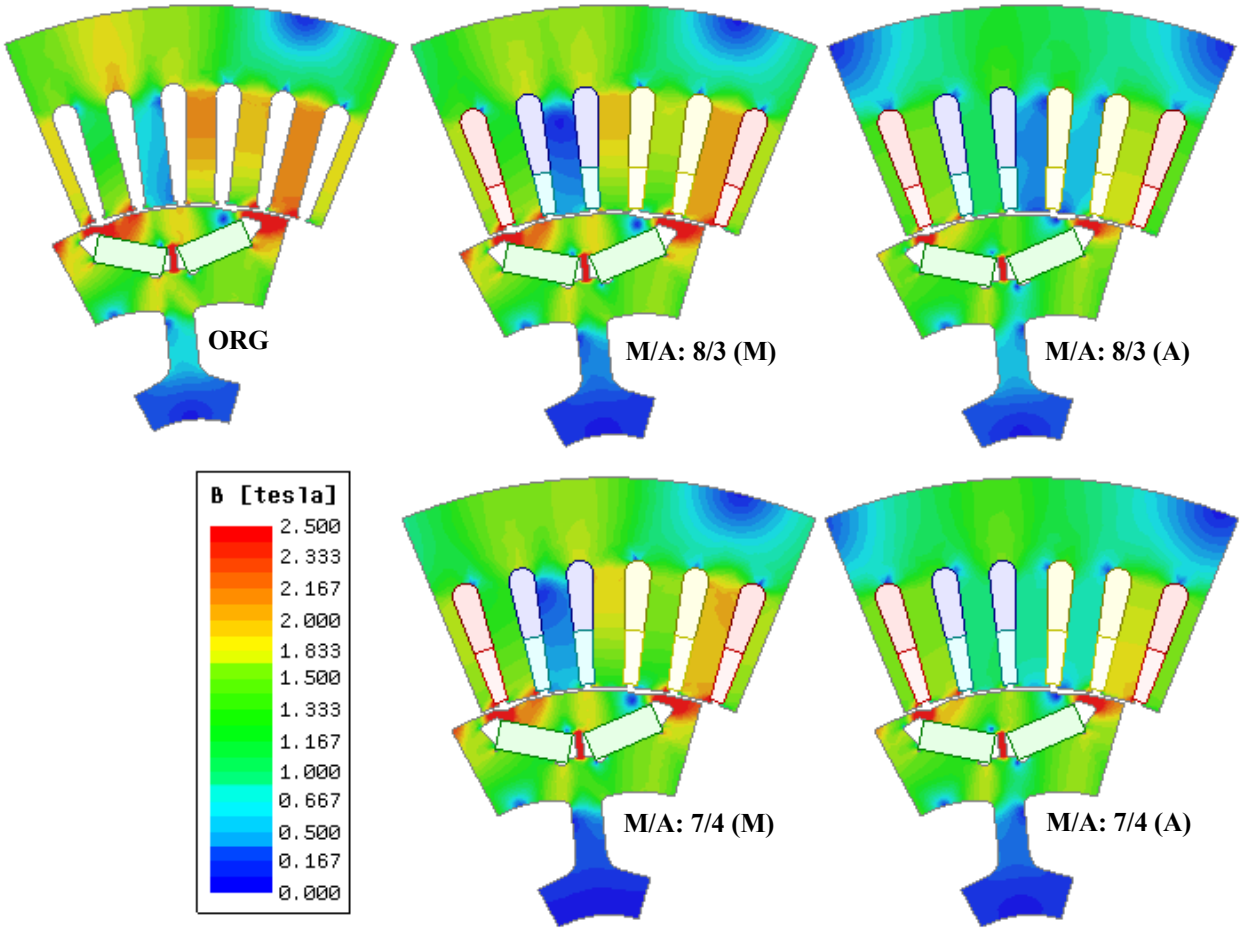

Figure 10 Flux density distributions.

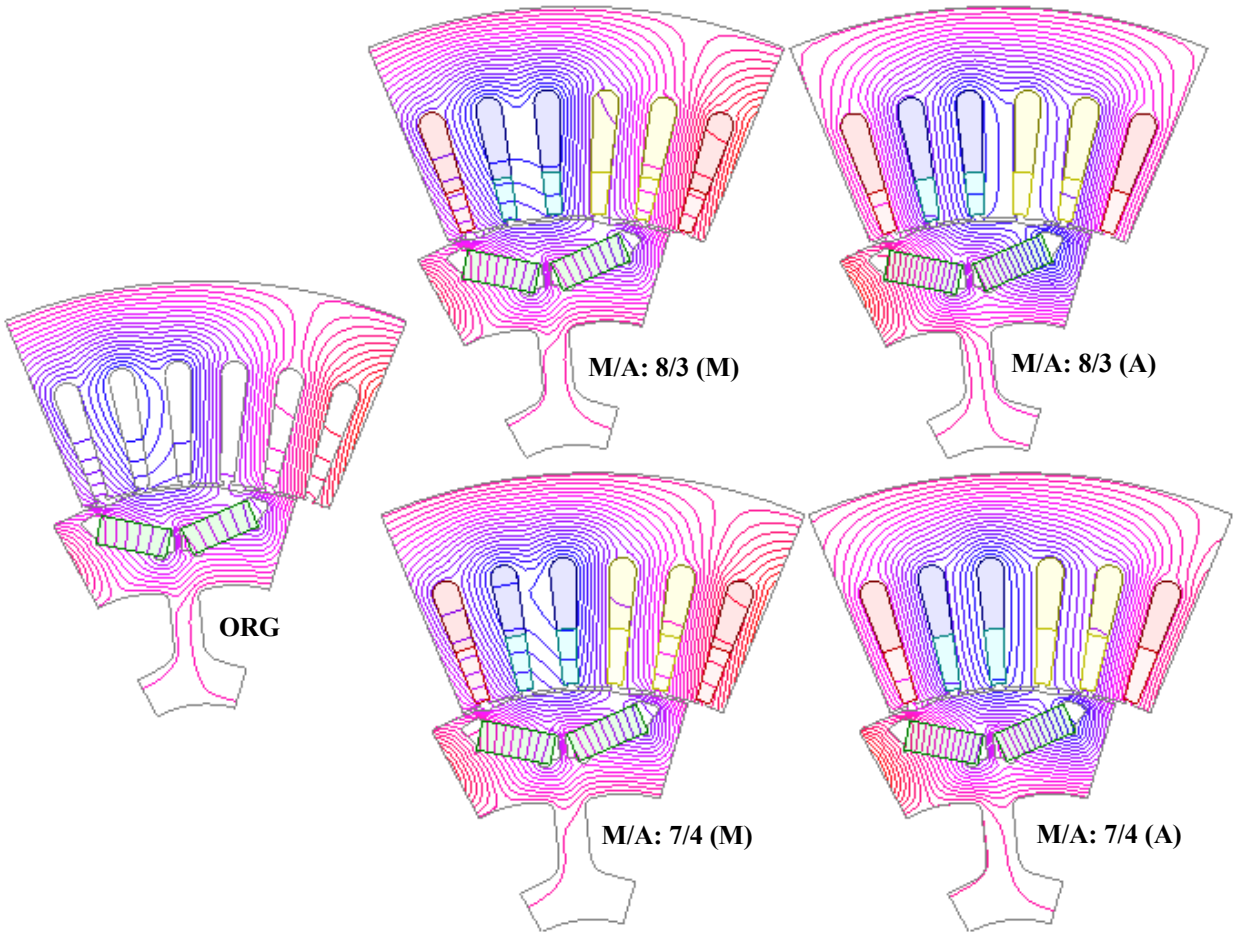

Figure 11 Flux line distributions.

Table 2 Comparison of key performance characteristics.

	ORG	**M/A: 8/3 and M/A: 7/4**			
		M8	***A3***	***M7***	***A4***
I_s (Apeak)	236				
n_s (rpm)	1000				
J_s (A/mm^2)	27.36				
Cur. Ang. (Deg.)	45	40	25	40	30
N_{ts}	11	8	3	7	4
N_{cs}	8				
N_{tp}	88	64	24	56	32
At	1836	1335	501	1168	668
R_{phase} (@21°C) (Ω)	0.077	0.0576	0.0194	0.0508	0.0262
k_f (%)	0.4482				
T (Nm) @	238.28	184.72	72.46	165.13	100.42
ΔT (%)	10.23	8.39	5.08	7.26	6.22
P_{out} (kW)	25.04	19.33	7.58	17.28	10.5
η (%)	78.68	84.51	69.12	84.63	77.53

5. Analysis of FW Characteristics

This section explored the effect of the number of turns on the FW performance of the considered IPM machines. Torque-speed, power-speed, and efficiency characteristics of the Toyota Prius 2010 IPM machine and its number of changing versions with different number of turns combinations per main and auxiliary windings have been investigated in this section. Since the ORG and M+A designs have the same total number of turns (i.e. 11-turns per slot) and geometric parameters, their electromagnetic properties are identical. The FW characteristics of the ORG and turn-changing designs have been compared as illustrated in Figure 12. As seen in the figure, thanks to the proposed method, it is possible to increase the torque and hence the power significantly at constant power and deep-flux weakening-regions. If the Toyota Prius IPM machine is designed with 8-turn main and 3-turn auxiliary windings M/A: 8/3, 275% higher power than that of the original design can be achieved in the deep FW region. If higher torque and power are required at the mid-constant-power region, then it is reasonable to design the windings with 7-turn and 4-turn for main and auxiliary windings (M/A: 7/4), respectively.

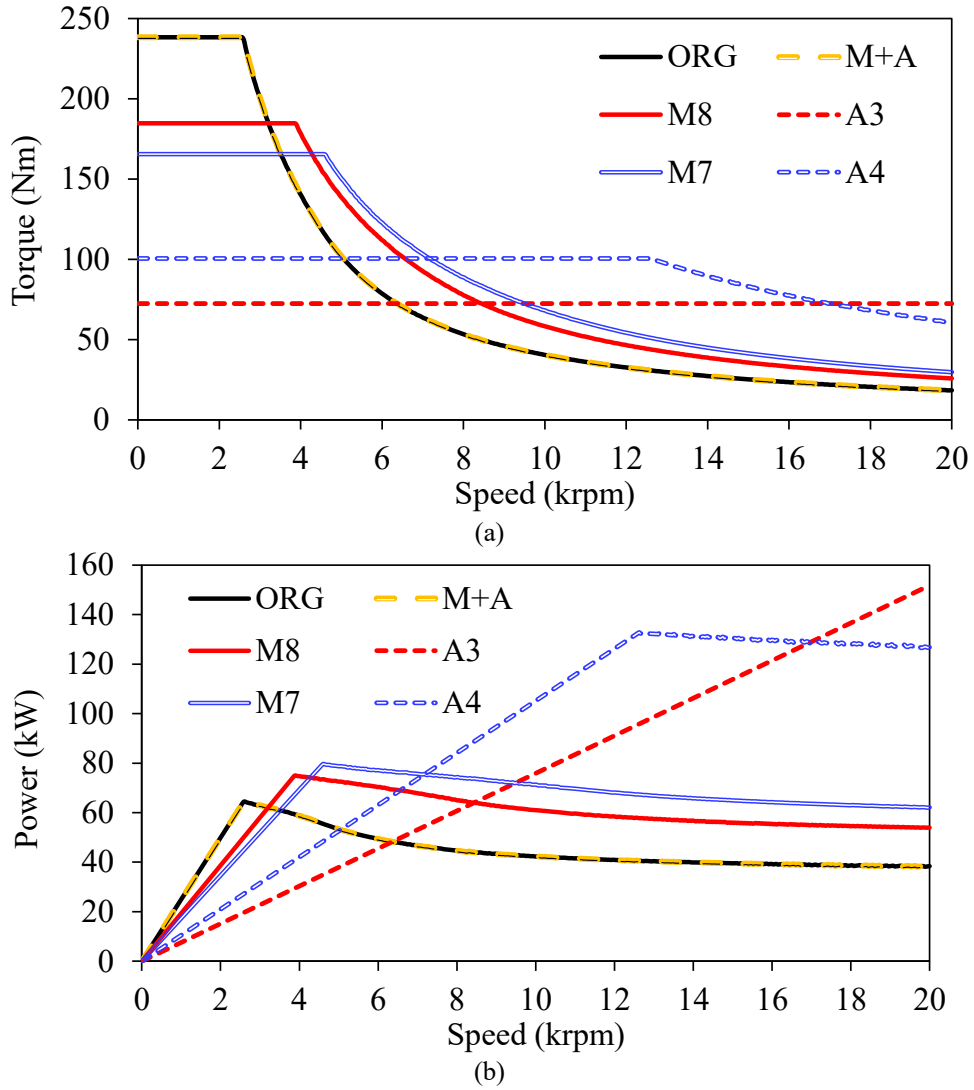

Figure 12 Comparison of FW performances of the IPM machines with different number of main and auxiliary turns.

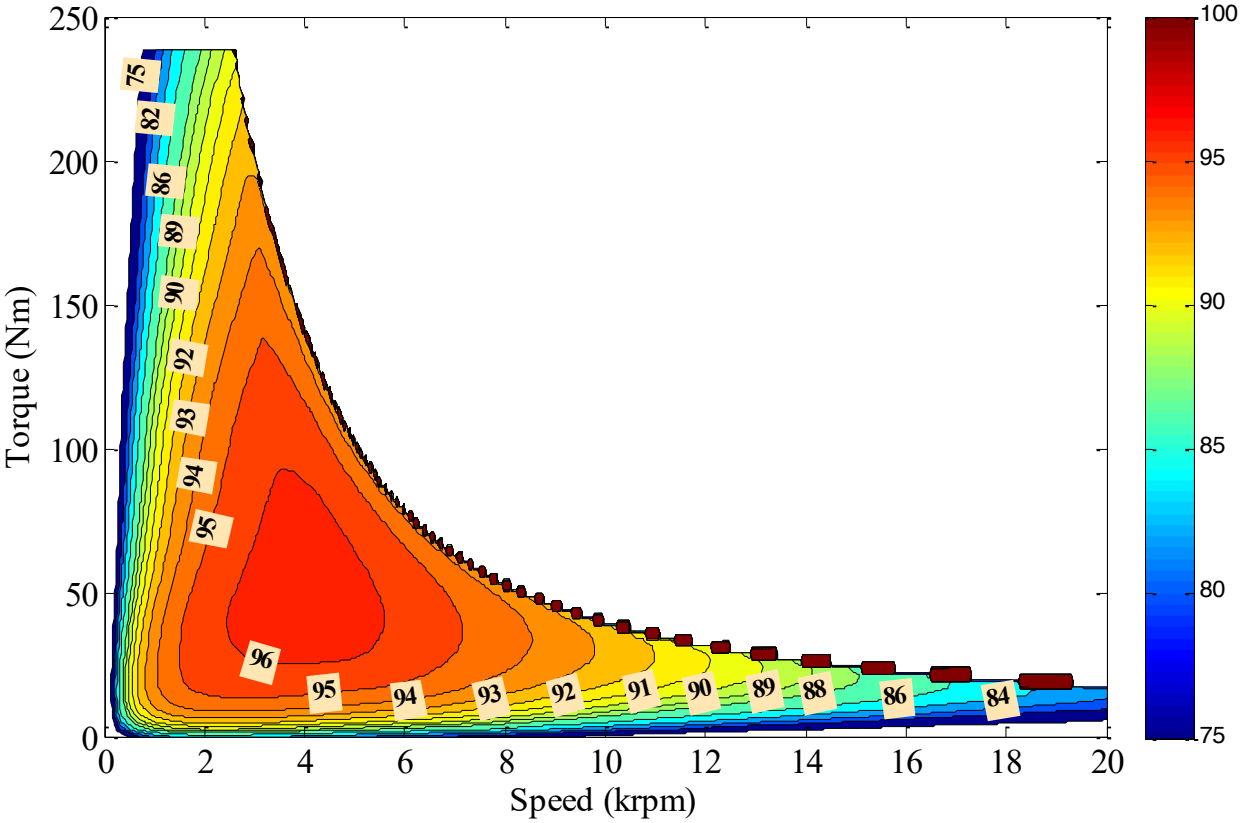
Torque (Nm)
Speed (krpm)
0
50
100
150
200
250
0
2
4
6
8
10
12
14
16
18
20
75
82
86
89
90
92
93
94
95
96
95
94
93
92
91
90
89
88
86
84
100
95
90
85
80
75

(a) ORG

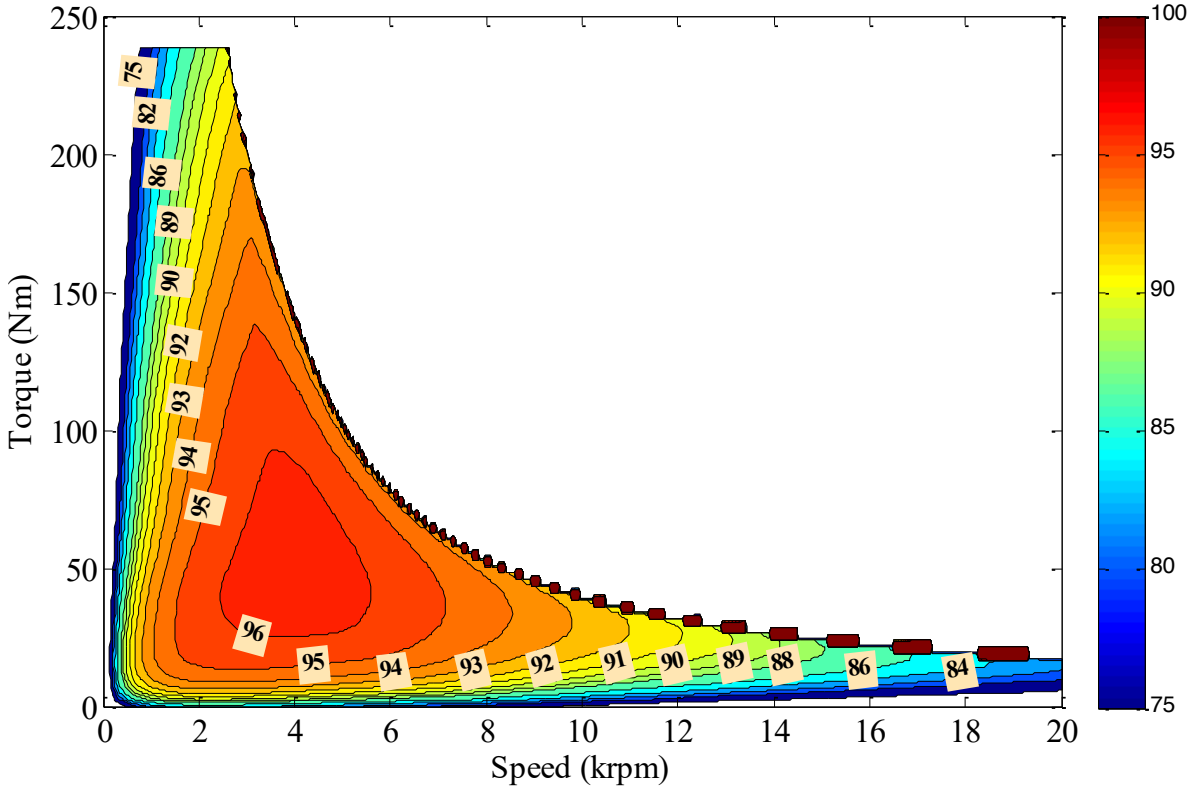
Torque (Nm)
Speed (krpm)
0
50
100
150
200
250
0
2
4
6
8
10
12
14
16
18
20
75
82
86
89
90
92
93
94
95
96
95
94
93
92
91
90
89
88
86
84
100
95
90
85
80
75

(b) M+A

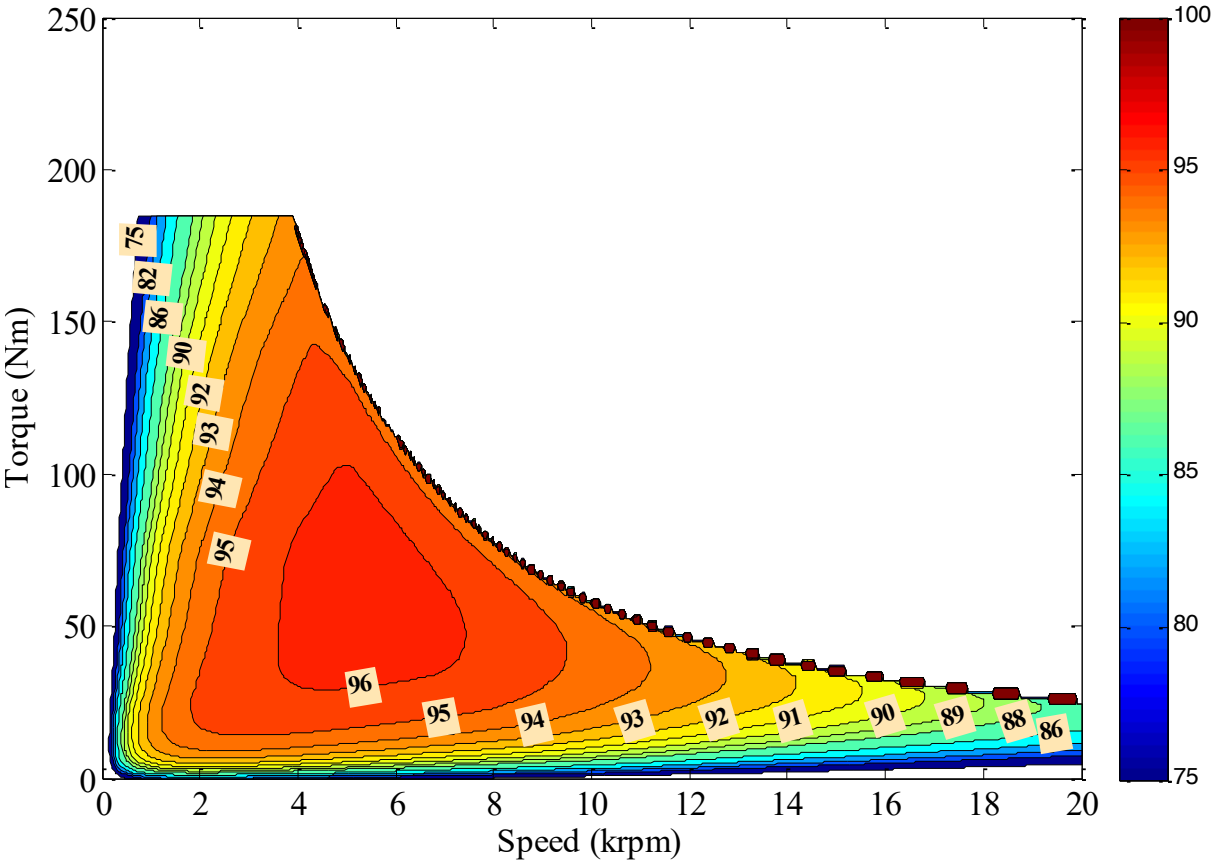
Torque (Nm)
Speed (krpm)
250
200
150
100
50
0
0
2
4
6
8
10
12
14
16
18
20
75
82
86
90
92
93
94
95
96
95
94
93
92
91
90
89
88
86
100
95
90
85
80
75

(c) M8

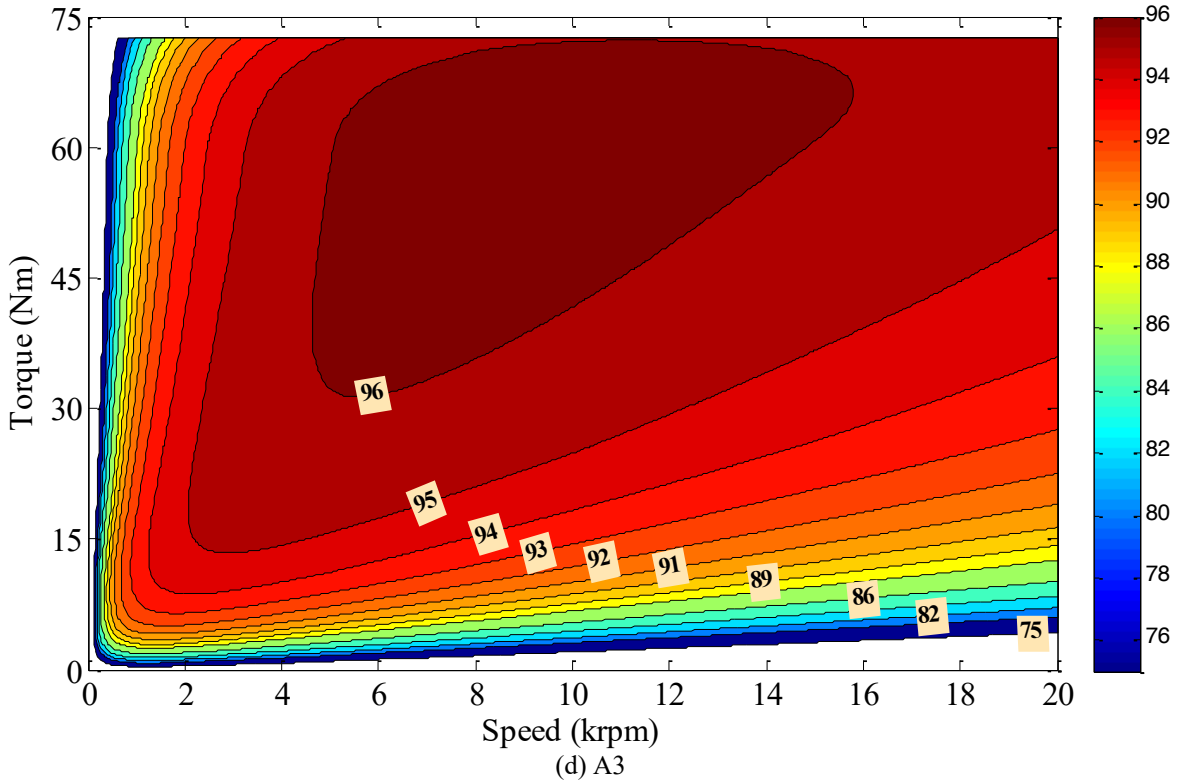
Torque (Nm)
Speed (krpm)
75
60
45
30
15
0
0
2
4
6
8
10
12
14
16
18
20
96
95
94
93
92
91
89
86
82
75
96
94
92
90
88
86
84
82
80
78
76

(d) A3

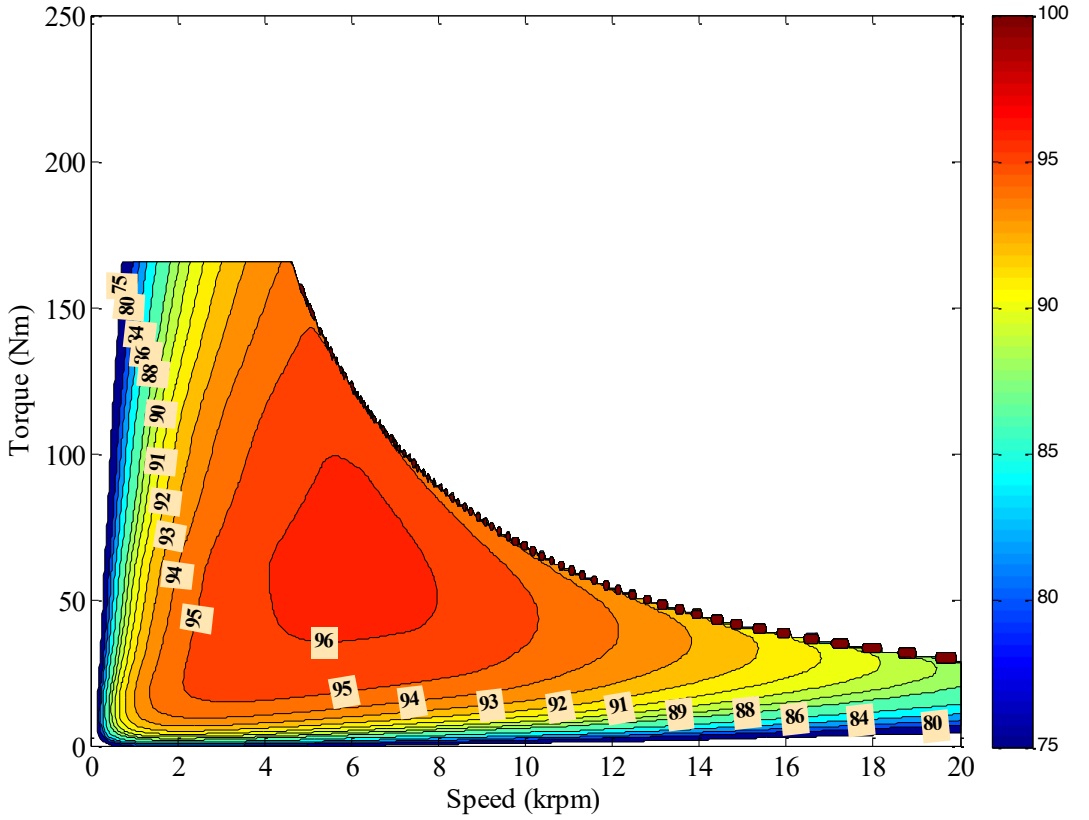

(e) M7

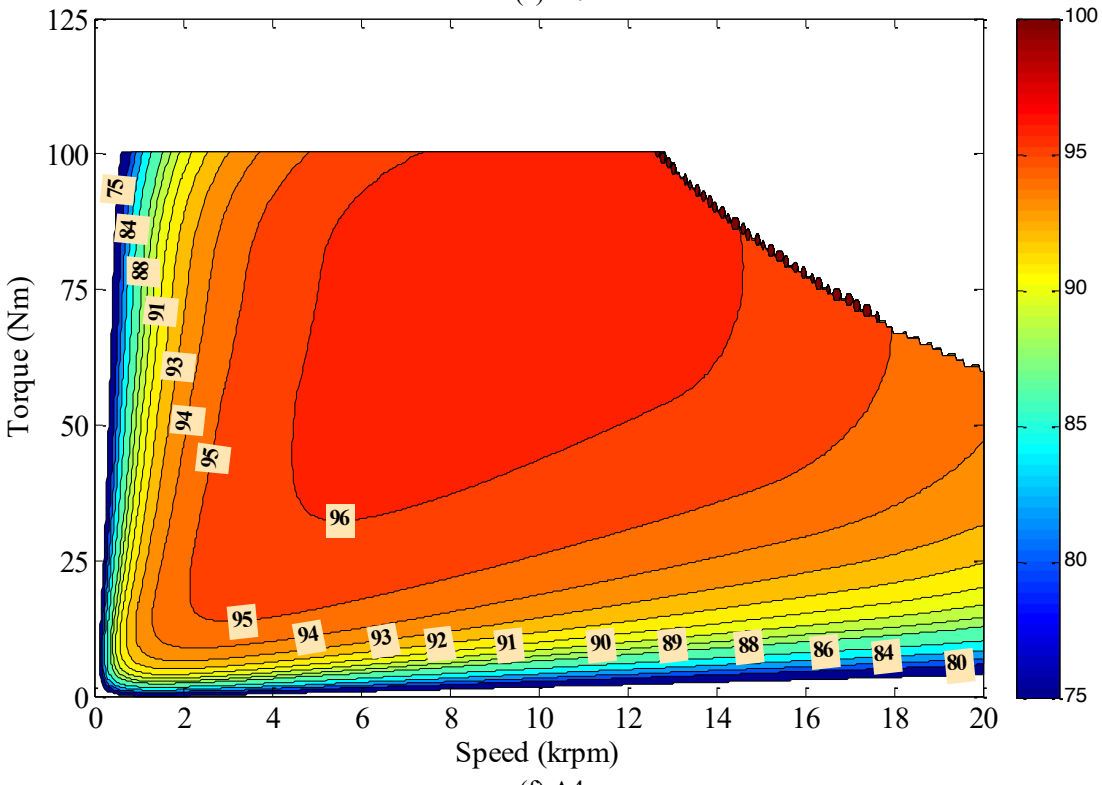

(f) A4

Figure 13 Comparison of efficiency maps of conventional and new IPM machines with different number of turn concept.

The calculated efficiency maps are illustrated in Figure 13. Mechanical losses, in addition to copper and core losses, have been considered during efficiency map calculations. Moreover, the winding resistor has been calculated for 100°C for the calculation of copper losses. It can be deduced that the suggested strategy has greatly improved the efficiency in high speed regions. Note that, in order to increase the efficiency at the low-speed and low-torque regions further, the diameter of the main and auxiliary windings should be increased together. Moreover, increasing the slot fill factor will also help to increase the overall efficiency. Alternatively, the efficiency of the mid-constant power and/or deep FW regions can be increased by changing the diameters of the main and auxiliary windings. However, this would cause a decrease in the efficiency in the constant-torque region. As shown in Figure 14, the performance characteristics of the designs' individual main and auxiliary winding activations have been integrated in order to evaluate the designs' whole-working condition. If the winding switches were activated at the correct time, the FW performance of the Prius IPM machine could be improved significantly thanks to the proposed turn-changing method.

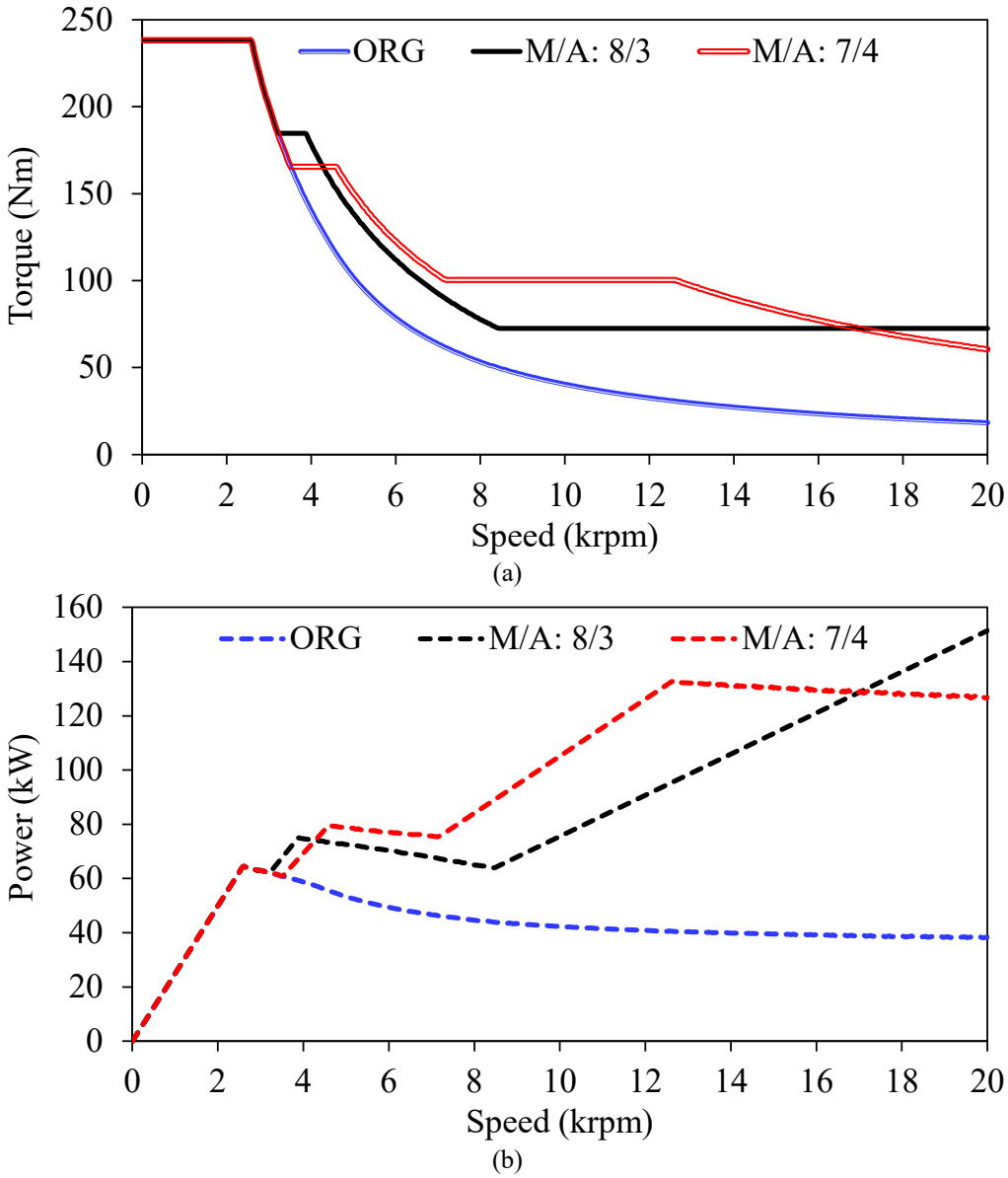

Figure 14 Comparison of torque- and power-speed characteristics of conventional (ORG), and new (M8/A3) and (M7/A4) IPM machines with number of turns switching concepts.

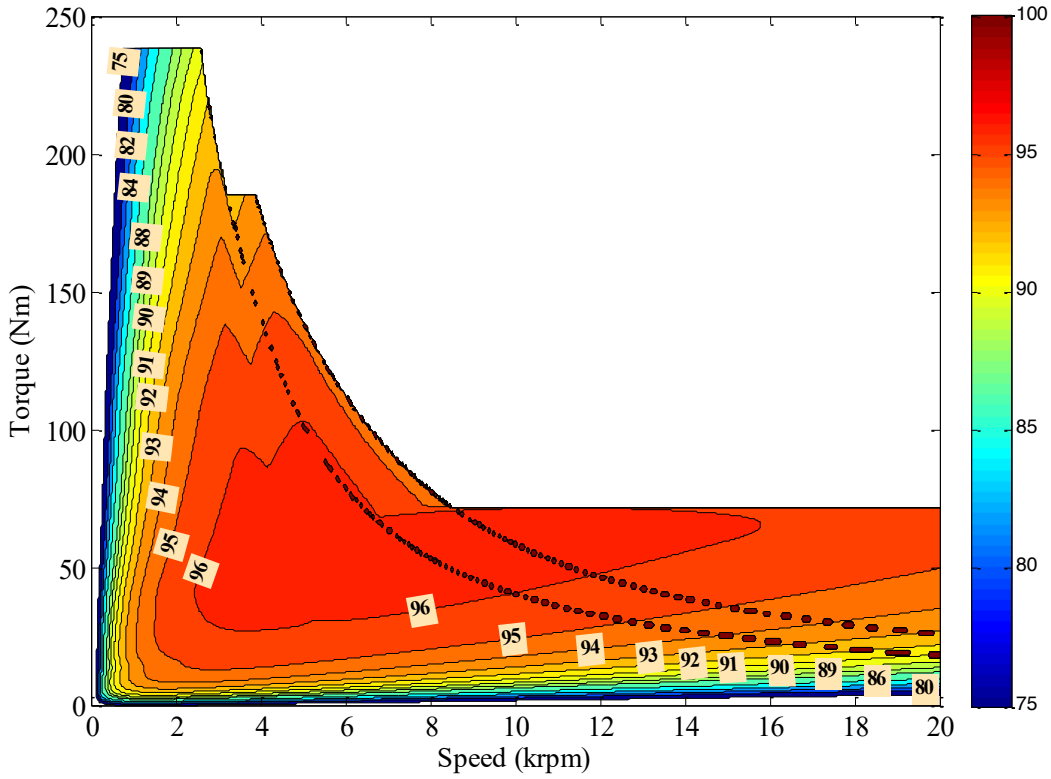

(a) M8/A3

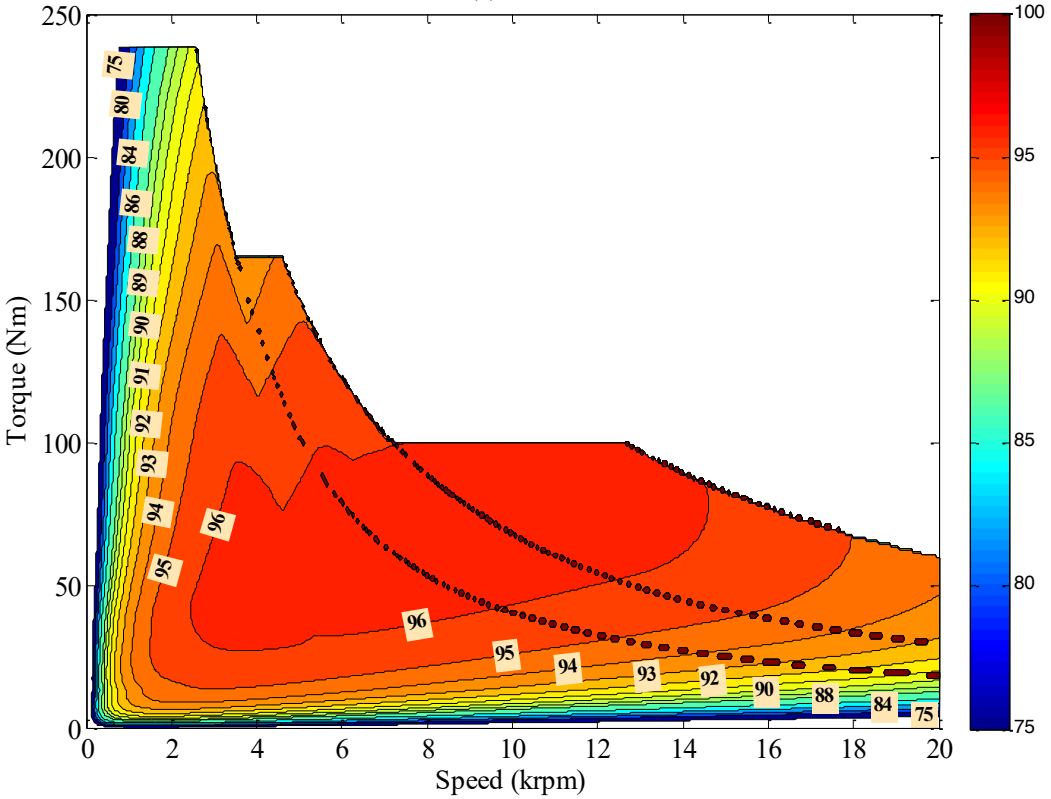

(b) M7/A4

Figure 15 Comparison combined efficiency maps.

The combined versions of the efficiency maps are shown in Figure 15. The efficiency at constant power and in deep FW regions is fairly good in both scenarios, as indicated in the figure (M/A: 8/3 or M/A: 7/4). Conclusion: The deeper the FW region and the constant power region, the higher the torque, the better the efficiency.

Phase current and voltage changes with respect to speed are shown in Figure 16 to demonstrate that the current and voltage limitations have not been exceeded. It is clear that no operating point has exceeded the current or voltage restrictions. As a consequence, the torque and power in the high-speed operation areas may be greatly improved thanks to the turn number changing idea without going above the current and voltage restrictions of the inverter.

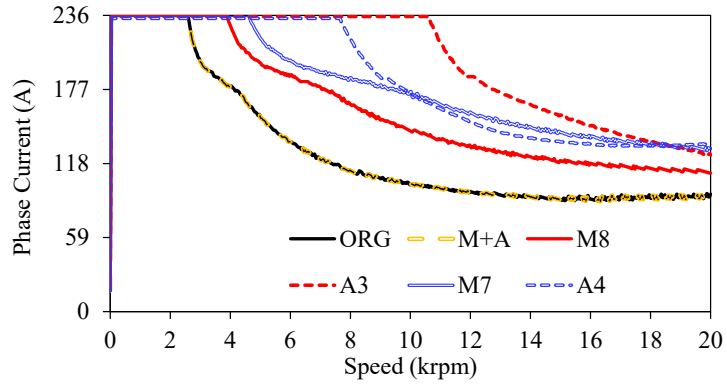

(a) Phase current

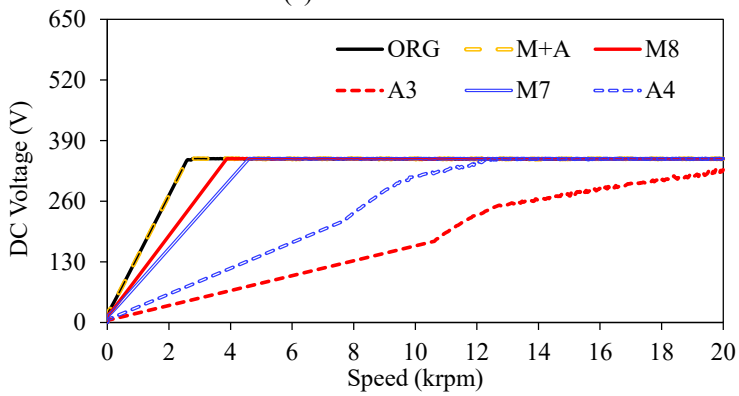

(b) Inverter voltage ($U_{dc} = 2 \times 0.85 \times U_{max}/\pi$)

Figure 16 Variation of phase current and inverter DC voltage with respect to speed.

6. FW Characteristics Verification

In order to validate that the FW performance calculations are correct, the calculated FW performance of the Toyota Prius IPM machine with 236Apeak phase current and 650V×2×0.85/π inverted voltage has been compared with the measured characteristics. The measurement results have been taken from the reports of Oak Ridge National Laboratory [39]. The calculated FW performance of the Prius IPM machine under the operation conditions given above is shown in Figure 17. As seen in the figure, the peak torque is about 238Nm and the peak power is 60kW.

The calculated and measured efficiency maps of the Prius IPM machine are illustrated in Figure 18. It is obvious that the measured efficiency map is obtained under lower phase current injection operation However, as demonstrated in the Prius IPM machine's locked rotor test [39], the peak torque is approximately 200Nm when operating at 200A current.

As seen in the figure, the peak efficiency is 96% between about 2.5 and 6 krpm and 4.5 and 6.5krpm for calculated and measured, respectively. Furthermore, the operation region's efficiency levels exceeding 88 percent are dispersed throughout a considerable portion of the territory. It is obvious that operations using more current at the same number of phase turns cost less efficiently. However, as shown in Figure 13(c), when the number of turns is reduced from 11 to 8, an almost identical efficiency map to the measured one is obtained.

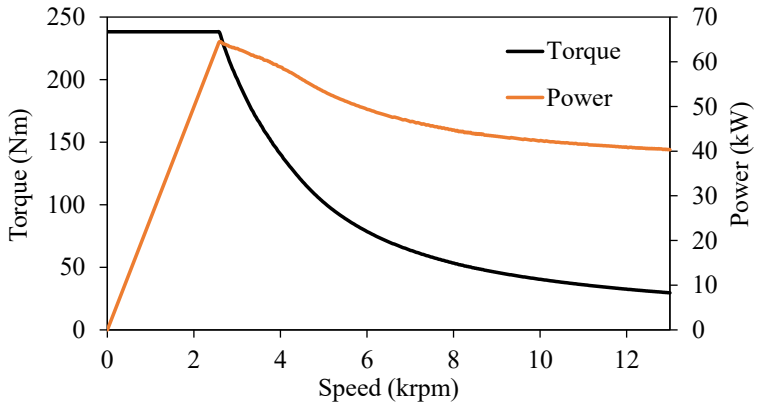

Figure 17 Torque- and power-speed characteristics of Prius IPM for 236A and 650V×2×0.85/π.

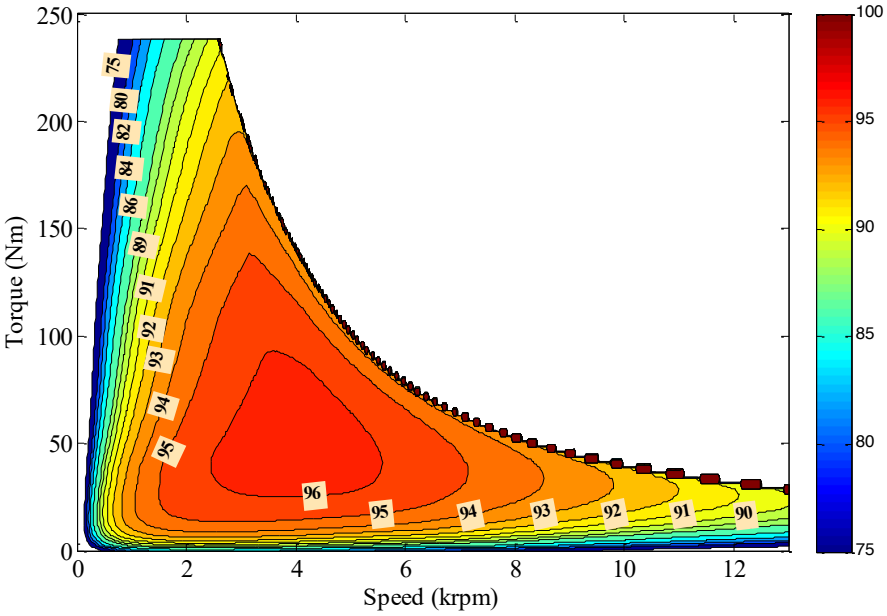

(a) Calculated efficiency map.

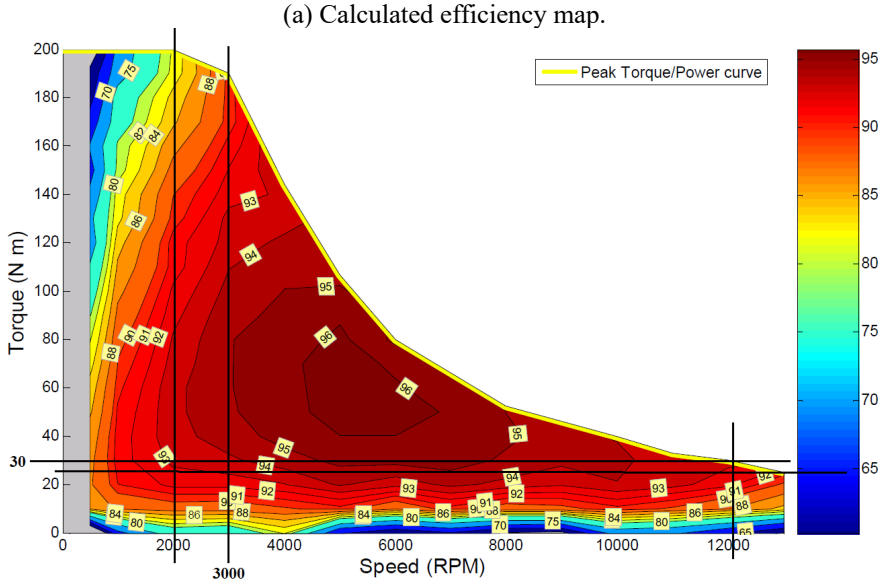

(b) Measured efficiency map [39].

Figure 18 Comparison of calculated and measured efficiency maps for Toyota Prius 2010 IPM machine.

7. Conclusions

This paper proposes and implements an unconventional winding-switching approach in IPM machines to improve FW capability and efficiency. The basic structure and working principle of the considered topology are explained. The main and auxiliary windings are activated based on the torque demand by simply changing the status of switches. Thus, the steady-state and FW performance of IPM machines having different number of turns in their main and auxiliary windings have been investigated in depth. The IPM machine topologies having winding-switching features are compared with Toyota Prius IPM machine's performance characteristics in order to reveal the merits/demerits of the proposed methodology. The following advantages have been achieved over the conventional IPM by implementing the proposed winding-switching approach to the IPM machines.

- Ability to adjust flux as a wide range: wide FW capability;
- Significantly improved FW performance characteristics: substantially high power at high speed;
- Move the highest efficient region from the high torque to the low torque at the constant torque region;
- Move the highest efficient region from the high speed to the low-speed operating region;
- Overall high efficiency.

Moreover, the predicted efficiency map of the original Toyota Prius 2010 IPM machine is verified using the efficiency measurements provided to ensure the accuracy of the analytical and numerical calculations offered in this work.

References

[1] Jans TM. Flux-weakening regime operation of an interior permanent magnet synchronous motor drive. IEEE Trans. Ind. Appl. 1987; IA-23(4): 681-689.

[2] Sebastian T, Siemon GR. Operating limits of inverter-driven permanent magnet motor drives. IEEE Trans. Ind. Applicat. 1987; 23: 327-333.

[3] Schiferl RF, Lipo TA. Power capability of salient pole permanent magnet synchronous motor in variable speed drive applications. IEEE Trans. Ind. Applicat. 1990; 26: 115-123.

[4] Sneyers B, Novotny DW, Lipo TA. Field weakening in buried permanent magnet Ac motor drives. IEEE Trans. Ind. Applicat. 1985; 21: 398-407.

[5] Lawler S, Bailey M, McKeever W. Extended constant power speed range of the brushless DC motor through dual mode inverter control. 2001. Oak Ridge National Lab., UT-Battelle, LLC, USA.

[6] Bailey M, et al. Dual mode inverter control test verification. 2001. Oak Ridge National Lab., UT-Battelle, LLC, ORNUTM-20001172.

[7] Ostovic V. Memory motors-a new class of controllable flux PM machines for a true wide speed operation. In: IEEE Ind. Appl. Conf.; Oct. 2001; Chicago, IL, USA. pp. 2577-2584.

[8] Hemmati S, Barigh M. A new approach for field weakening in a surface mounted permanent magnet synchronous motor by winding switching. 27th Iranian Conf. Elect. Eng. (ICEE'19); May 2019; Yazd, Iran. pp. 509-514.

[9] Hemmati S, Lipo TA. Field weakening of a surface mounted permanent magnet motor by winding switching. Int. Symp. Power Electron, Elect. Drives, Auto. Motion; Jun. 2012; Sorrento, Italy. pp. 736-740.

[10] Sin S, Roshanzamir A, Kwon B. I. Improvement of the Constant-Power Speed Range of Surface-Permanent Magnet Machine Using Winding Switching. IEEE Access 2021; 9: 32298-32309.

[11] Im SH, Park GM, Gu BG. Novel Winding Changeover Method for A High Efficiency AC Motor Drive. IEEE Energy Convers. Cong. Expo. (ECCE'19); Oct. 2019; Baltimore, MD, USA. pp. 2347-2352.

[12] Vido L, Amara Y, Gabsi M, Lecrivain M, Chabot F. Compared performances of homopolar and bipolar hybrid excitation synchronous machines. Proc. IEEE Ind. Appl. Conf.; Oct. 2005; Hong Kong, China. pp. 1555–1560.

[13] Vido L, Amara Y, Gabsi M, Lecrivain M, Chabot F. Homopolar and bipolar hybrid excitation synchronous machines. IEEE Int. Conf. Elect. Mach. Drives; May 2005; San Antonio, TX, USA. pp. 1212–1218.

[14] Chan CC, Chau KT, Jiang JZ, Xia W, Zhu M, Zhang R. Novel permanent magnet motor drives for electric vehicles. IEEE Trans. Ind. Electron., 1996; 43(2): 331–339.

[15] Tapia JA, Leonardi F, Lipo TA. Consequent-pole permanent magnet machine with extended field-weakening capability. IEEE Trans. Ind. Appl. 2003; 39(6): 1704–1709.

[16] Luo X, Lipo TA. A synchronous/permanent magnet hybrid AC machine. IEEE Trans. Energy Convers. 2000; 15(2): 203–210.

[17] Fodorean D, Djerdir A, Viorel IA, Miraoui A. A double excited synchronous machine for direct drive application—Design and prototype tests. IEEE Trans. Energy Convers. 2007; 22(3): 656–665.

[18] Li Y, Lipo T. A. A doubly salient permanent magnet motor capable of field weakening. Proc. IEEE Power Electron. Spec. Conf.; Jun. 1995; Atlanta, GA, USA. pp. 565–571.

[19] Kosaka T, Kano Y, Matsui N, Pollock C. A novel multi-pole permanent magnet synchronous machine with SMC bypass core for magnet flux and SMC field-pole core with toroidal coil for independent field strengthening/weakening. Proc. Eur. Conf. Power Electron. Appl.; Sep. 2005; Dresden, Germany. pp. 1–10.
[20] Zhu ZQ, Al-Ani M. MJ, Liu X, Lee B. A Mechanical Flux Weakening Method for Switched Flux Permanent Magnet Machines. IEEE Trans. Energy Convers 2015; 30(2): 806-815.
[21] Capponi FG, Donato G, Caricchi F. Recent advances in axial-flux permanent-magnet machine technology. IEEE Trans. Ind. Appl. 2012; 48(6): 2190–2205.
[22] Capponi FG, Terrigi R. Caricchi F, Ferraro L. Active output voltage regulation for an ironless axial-flux PM automotive alternator with electromechanical flux weakening. IEEE Trans. Ind. Appl. 2009; 45(5): 1785–1793.
[23] Zhou G, Miyazaki T, Kawamata S, Kaneko D, Hino N. Development of variable magnetic flux motor suitable for electric vehicle. In: Proc. Int. Power Electron. Conf.; Jun. 2010; Sapporo, Japan. pp. 2171–2174.
[24] Lei M, Sanada M, Morimoto S, Takeda Y, Matsui N. High efficiency adjustable speed control of IPMSM with variable permanent magnet flux linkage. In: Proc. Conf. Rec. IEEE IAS Annu. Meeting; Oct. 1999; Phoenix, AZ, USA. pp. 881–887.
[25] Lei M, Sanada M, Morimoto S, Takeda Y. Advantages of IPMSM with adjustable PM armature flux linkage in efficiency improvement an operating range extension. In: Proc. Power Convers. Conf.; Apr. 2002; Osaka, Japan. pp. 136–141.
[26] Kou B, Li C, Cheng S. Flux-weakening-characteristic analysis of a new permanent-magnet synchronous motor used for electric vehicles. IEEE Trans. Plasma Sci. 2011; 39(1): 511–515.
[27] Shakal A, Yuefeng L, Lipo TA. A permanent magnet AC machine structure with true field weakening capability. In: Proc. IEEE Int. Symp. Ind. Electron.; Jun. 1993; Budapest, Hungary. pp. 19–24.
[28] Ostovic V. Memory motor. IEEE Trans. Ind. Appl. 2003; 9(1): 52–61.
[29] Ostovic V. Pole-changing permanent magnet machines. IEEE Trans. Ind. Appl. 2002; 38(6): 1493–1499.
[30] Hengchuan L, Heyun L, Zhu ZQ, Mingming H, Ping J. Permanent magnet remagnetizing physics of a variable flux memory motor. IEEE Trans. Magn. 2010; 46(6): 1679–1682.
[31] Yu C, Chau K.T. Design, analysis, and control of DC-excited memory motor. IEEE Trans. Energy Convers. 2011; 26(2): 479–489.
[32] Yu C, Chau KT, Liu X, Jiang JZ. A flux-mnemonic permanent magnet brushless motor for electric vehicles. IEEE J. Appl. Phys. 2008; 103(7): 103–106.
[33] Swamy MM, Kume T, Maemura A, Morimoto S. Extended high speed operation via electronic winding-change method for AC motors. IEEE Trans. Ind. Appl. 2006; 42(3): 742–752.
[34] Ilhan E, Gysen BLJ, Paulides JJH, Lomonova EA. Analytical hybrid model for flux switching permanent magnet machines. IEEE Trans. Magn. 2010; 46(6): 1762–1765.
[35] Copt F, Raujo DM, Koechli C, Perriard Y. Current control strategy for dynamic winding reconfiguration of slotless brushless DC motors. IEEE Trans. Ind. Appl. 2019; 55(1): 417–425.
[36] Im SH, Gu BG. A snubberless solid-state tap changer for permanent magnet synchronous motors. IEEE Trans. Power Electron. 2020. 35(11): 12143–12152.
[37] He S, Li Q, Tong R, Shi G. Transformer economic operation control system based on zero-crossing switching; In: IEEE Advanced Inform. Technol. Electron. Autom. Control Conf. (IAEAC'15); Dec. 2015; Chongqing, China. pp. 508-512.
[38] Nian H, Zhou Y. Investigation and Suppression of Current Zero Crossing Phenomenon for a Semicontrolled Open-Winding PMSG System. IEEE Trans. Power Electron. 2017; 32(1): 602-612.
[39] Olszewski M. Evaluation of the 2010 Toyota Prius hybrid synergy drive system. 2011; Oak Ridge Nat. Lab. U.S. Dept. Energy.
[40] Gundogdu T. Design and Analysis of Double Fed Interior Permanent Magnet Machines for Traction Applications. In: 2022 IEEE IAS Global Conf. Emerging Technol. (GlobConET'22); May 2022; Arad, Romania. pp. 1-8.
[41] Gundogdu T, Komurgoz G. Influence of design parameters on flux-weakening performance of interior permanent magnet machines with novel semi-overlapping windings. IET Elect. Power Appl. 2020; 14: 2547-2563.